České vysoké učení technické v Praze
Fakulta elektrotechnická

Czech Technical University in Prague
Faculty of Electrical Engineering

Ing. Zdeněk Hurák, Ph.D.

Inerciální stabilizace optoelektronických systémů pro letecké prostředky

Inertial stabilization of airborne optoelectronic systems

Summary

The lecture gives an overview of results achieved by the author and his students in engineering research and development in the area of inertial stabilization of optoelectronic payloads for aerial surveillance. The results have been achieved during a series of joint projects with Czech Air Force and Air Defense Technological Institute (VTÚLaPVO in Czech), ESSA company, and Center for Machine Perception (CMP) at Faculty of Electrical Engineering at CTU in Prague. Although the focus of all those projects was on development of real commercializable devices, we succeeded in identifying a few general problems at the intersection of control engineering and robotics, for which we consequently proposed novel solutions, presented these at prestigious international conferences and published in leading journals such as IEEE Transactions on Control Systems Technology. In this lecture, after explaining the very basics of inertial stabilization, it will be shown how the inertial stabilization loops for the common double-gimbal system can be augmented with automatic visual tracking loops. A compensation scheme for delay in the visual tracking loop will also be explained. Finally, the usefulness of advanced computational design routines for controllers of a given order and structure will be demonstrated. The actual lecture is accompanied by a few videos from flight tests onboard helicopters.

Souhrn

Přednáška podává přehled výsledků dosažených autorem a jeho studenty ve výzkumu a vývoji v oblasti inerciální stabilizace optoelektronických systémů pro pilotované i bezpilotní letecké prostředky. Tyto výsledky byly získány během série společných projektů s Vojenským technickým ústavem letectva a protivzdušné obrany (VTÚLaPVO), pražskou strojírenskou firmou ESSA a výzkumným týmem z Centra strojového vnímání (CMP) z Fakulty elektrotechnické ČVUT v Praze. Jakkoliv byly tyto projekty zaměřeny na vývoj reálných komercializovatelných systémů, podařilo se také identifikovat několik zobecnitelných problémů na pomezí teorie automatického řízení a robotiky, které byly následně inovativně vyřešeny a řešení prezentována na prestižních mezinárodních konferencích i ve špičkových časopisech typu IEEE Transactions on Control Systems Technology. V přednášce bude po podání úvodu do problematiky inerciální stabilizace vysvětleno, jak lze rozšířit inerciálně-rychlostní stabilizační smyčku pro dvojzávěsový kamerový systém o zpětnou vazbu od obrazu, jak lze kompenzovat zpoždění v obrazové zpětné vazbě i jak lze s výhodou využít moderních výpočetních nástrojů pro návrh robustních řídicích systémů se zadanou strukturou. V samotné přednášce bude předvedeno i několik videí demonstrujících funkčnost systému v reálném provozu na helikoptéře.

Klíčová slova

inerciální stabilizace; směr pohledu; letecké sledování; řízení pohybu; obrazové sledování

Keywords

inertial stabilization; line of sight; aerial surveillance; motion control; visual servoing

Contents

1 Introduction

1.1 Inertial line-of-sight stabilization on mobile carriers

The very basic control task for steerable cameras or antennas mounted on mobile carriers such as trucks, unmanned aircraft or ships, is to keep the commanded line of sight (optical axis) still even in presence of various disturbing phenomena like mass disbalance, aerodynamic (or wind-induced) torque and possible kinematic coupling between gimbal axes, see Fig.1. Motivated also by defense technological needs, the topic of inertial stabilization was studied extensively in the past few decades. Several relevant papers from 1970s through 1990s were archived in the selection [1]. Dedication of a full issue of *IEEE Control System Magazine* (February 2008) featuring nice survey papers [2], [3] and [4] confirms that the topic is still relevant for the engineering community. Another recent issue of the same journal brings a rigorous analysis of control problems related to a standard double gimbal system [5], though it is not directly applicable to inertial stabilization.

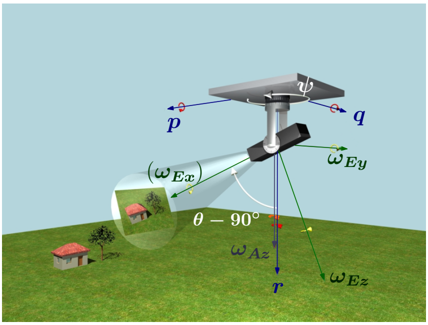

Figure 1: Basic scenario for inertial line-of-sight stabilization. Green are the components $\omega_{Ex}, \omega_{Ey}, \omega_{Ez}$ of the vector of inertial angular rate of the elevation frame (as measured by MEMS gyros attached to the camera), blue vectors p, q, r denote the rate components of the base (UAV here). The ω_{Az} component is attached to the outer gimbal (the other two components are not shown). Two white arcs denote the two relative angles.

1.2 Automatic visual tracking on mobile carriers

All of the above cited works (including the references made therein) mostly focus on the task of inertial stabilization only. The issue of extending the inertial rate stabilizing feedback loop to visual tracking system is only dealt with at a rather simplistic level in [2] by suggesting the common cascaded control structure for every rotational degree of freedom: a single-input-single-output inner (inertial rate stabilization) loop is accepting commands from the output of the corresponding outer (visual tracking) loop. There are some pitfalls hidden in this decoupled approach, though. This paper will describe the troubles that are encountered when using the classical double-gimbal platform and offer a solution. To the best of the authors knowledge, this is the first formal treatment of visual pointing and tracking for inertially stabilized camera systems. Preliminary versions of this paper were presented at [6] and [7]; the present paper includes corrections and some minor theoretical extensions but the most important extension is in supporting the theoretical analysis by reporting on laboratory experiments with a realistic benchmark platform.

1.3 Experimental platform

The configuration considered in this study is the common two-degree-of-freedom configuration: double gimbal system. The inner gimbal allows for elevation of the payload, the outer gimbal allows for a change in heading (or azimuth) angle. A benchmark system was designed and built within a project coordinated by Czech Air Force and Air Defense Technological Institute (Vojenský ústav letectva a PVO) in collaboration with Czech Technical University in Prague and ESSA company. The payload consists of a regular RGB camera, infrared camera and laser range-finder, see Fig.2. Direct drive motors are used for the two axes and MEMS based gyros (inertial rate sensors) are attached to the payload.

1.4 Notation for coordinate frames and their rotations

The paper relies on expressing rotations of coordinate frames with respect to some other coordinate frames. The right-handed orthogonal

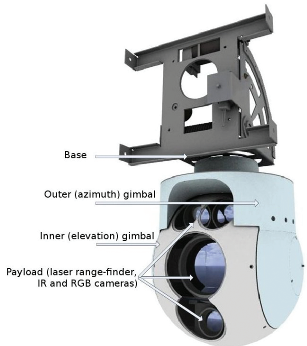

(a) 3D visualization: both the azimuth and the elevation angles can rotate $n \times 360°$.

(b) Real platform. The supporting structure is only used in a lab.

Figure 2: One of the platforms developed by VTÚLaPVO in collaboration with two teams of FEL ČVUT and ESSA company

coordinate frames are represented by triads of vectors $\{x, y, z\}$ and for simplicity they all assume a common origin; this is certainly justifiable when far-away objects are tracked. The coordinate frames and their symbols used in subscripts and superscripts are: the reference coordinate frame [R] aligned with the ground but translated to the center of gravity of the carrier, its z_R axis oriented towards the ground as is common in aerospace appplications; the base coordinate frame fixed to the body of the carrier [B] with its x_B axis heading forward and y_B to the starboard; the coordinate frame attached to the outer (azimuth) gimbal [A], which can rotate with respect to the carrier around the $z_B = z_A$ axis; the coordinate frame attached to the inner (elevation) gimbal [E], which can rotate with respect to the azimuth gimbal around the $y_A = y_E$ axis; and finally the coordinate frame attached to the camera [C]. Rotation of [C] with respect to [E] is fixed and is used just for the "esthetic" purpose of (re)denoting the camera optical axis as the z_C axis.

The sequence of the two key rotations expressing the pose of the inner gimbal (fixed to camera) with respect to the base (carrier) is visualized in Fig. 3 and for completenes it is given by

$$R_A^B = \begin{bmatrix} \cos\psi & -\sin\psi & 0 \\ \sin\psi & \cos\psi & 0 \\ 0 & 0 & 1 \end{bmatrix} \tag{1}$$

and

$$R_E^A = \begin{bmatrix} \cos\theta & 0 & \sin\theta \\ 0 & 1 & 0 \\ -\sin\theta & 0 & \cos\theta \end{bmatrix}, \tag{2}$$

where the lower and upper indices are used here as "rotation matrix expressing the coordinate triade of the A frame within the B frame". Applying the right-hand rule, the (outer) azimuth gimbal rotates to right for the positive angle ψ and the (inner) elevation gimbal rotates up for a positive increment in the θ angle. Using the common shorthand notation like $c_\psi = \cos\psi$, the composition of the two rotations is given by the matrix product

$$R_E^B = \begin{bmatrix} c_\psi c_\theta & -s_\psi & -c_\psi s_\theta \\ s_\psi c_\theta & c_\psi & -s_\psi s_\theta \\ -s_\theta & 0 & -c_\theta \end{bmatrix}. \tag{3}$$

Finally, the fixed rotation between the camera frame and the elevation frame is given by

$$R_C^E = \begin{bmatrix} 0 & 0 & 1 \\ -1 & 0 & 0 \\ 0 & -1 & 0 \end{bmatrix}. \tag{4}$$

When specifying angular rates, the subscript/superscript scheme used here follows the common style, defined for instance in [8]: one needs to tell which coordinate frame is rotating with respect to which other coordinate frame, and in which coordinate frame is such a vector expressed. For example, $\omega_{A,E}^R$ stands for the angular rate of the Elevation gimbal with respect to the Azimuth gimbal, expressed in the Reference frame. Oftentimes, the notation is relaxed in the paper to avoid cluttering the formulas with indices. For instance, ω_A is a short notation for $\omega_{R,A}^A$, that is, the inertial angular rate of the A gimbal. Its z component is then ω_{Az}.

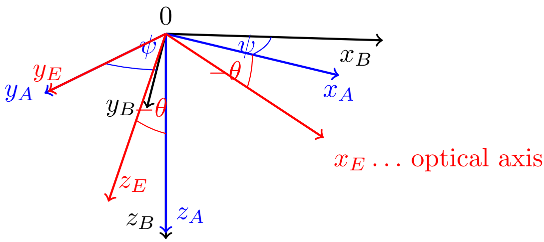

Figure 3: Composition of rotation of coordinate frames attached to the carrier (base), outer (azimuth) gimbal and inner (elevation) gimbal. The [C] frame attached to the camera not visualized here, see Fig.5.

2 Inertial rate stabilization

In order to make the line of sight insensitive to external disturbances, a simple controller structure can be used. Two decoupled SISO inertial rate controllers suffice, one for each measured (component of the) inertial angular rate. Namely,

- the inertial angular rate ω_{Ey} (also denoted with the mnemotechnic ω_{EL}) of the payload about the axis of the elevation motor (camera elevation rate),
- and the inertial angular rate ω_{Ez} of the payload around its own vertical axis, also nicknamed camera cross-elevation rate (and denoted ω_{CEL}) since its axis is always orthogonal to the ω_{EL} axis.

This is visualized in Fig.1. The resulting decoupled controller configuration is in Fig.4. It is clear from Fig.1 that the cross-elevation controller must include a secant gain correction $1/cos(\theta)$, because the motor in the azimuth gimbal cannot directly affect $\omega_{\mathrm{CEL}}(= \omega_{Ez})$. It can only do so indirectly through ω_{Az}. It is only when the camera is pointing to the horizon, that is, when $\theta = 0$, that $\omega_{Az} = \omega_{\mathrm{CEL}}(= \omega_{Ez})$. See [3] for details.

Even though there is some gyroscopic coupling between the two axes (see [9], [10] for full models or [5] for the simplified version when the base is still), its influence is not worth designing a MIMO rate controller.

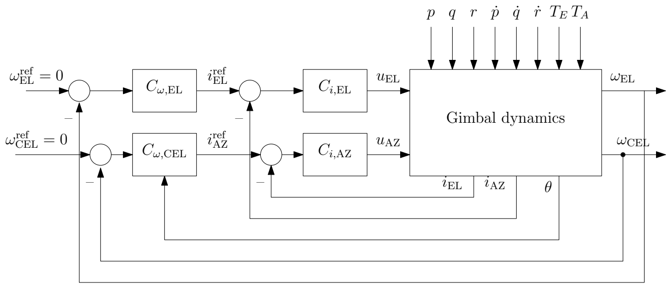

Figure 4: Inertial stabilization. Two independent (decoupled) SISO feedback loops, one for each rate gyro attached to the body of camera, $\omega_{\mathrm{EL}}(= \omega_{Ey})$ and $\omega_{\mathrm{CEL}}(= \omega_{Ez})$. The cross-elevation stabilizing controller must contain secant gain correction $1/cos(\theta)$. The disturbing variables are the carrier roll, pitch and yaw rates, p, q, r, respectively, their derivatives and external torques around the two motor axes. The innermost current loops are also depicted.

This neglected gyroscopic effect can be cast as yet another external disturbing torque and as such left to the rate controller to suppress.

3 Modeling for pointing and tracking

Before starting discussions on ways to design and implement a feedback controller for the task of pointing and tracking, a model must be developed. At the initial treatment, the inertial angular rate (feedback) loops can be regarded as perfect within the appropriate frequency range and saturation bounds, that is, the commanded inertial angular rates $\omega_{\mathrm{EL}}^{\mathrm{ref}}$ and $\omega_{\mathrm{CEL}}^{\mathrm{ref}}$ can be regarded as perfectly followed by the inner loops. To develop a mathematical model for this idealized situation, a few basic concepts from the established domain of visual servoing will be given. The next few paragraphs are fully based on the two chapters from [8] dedicated to computer vision and vision-based control. They are given here just for a convenience of a reader nonacquainted with these concepts. Another comprehensive introductory material is [11].

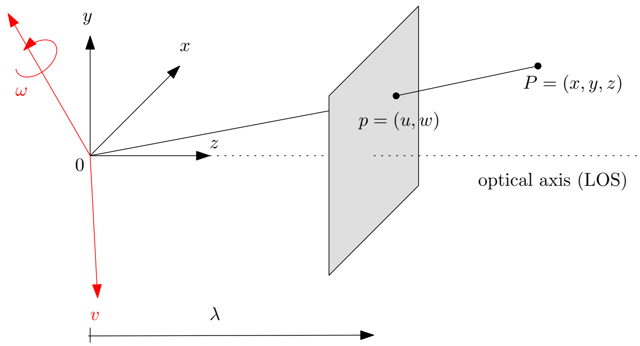

Figure 5: Coordinates of the object on the ground expressed in the coordinate frame attached to the camera and (after projection) in the image plane. Rotation $\omega_{R,C}^{C}$ and translation v_C of the camera frame within with respect to the inertial frame is also ilustrated (redrawn from [8]).

3.1 Perspective projection

The objects to be observed are located in the full 3D world while the camera can only record their 2D image. The coordinates of the object in the world (on the ground) expressed in the camera frame are given by $P = [x, y, z]^T$. Simplifying a bit the model of the optics, we make the so-called pinhole assumption, which defines the image coordinate frame as follows. At a focal distance λ from the origin of the camera coordinate frame, consider the image plane orthogonal to the optical axis of the camera. The coordinates of the point of intersection of the line connecting the object with the origin are $p = [u, w, \lambda]^T$. The vector $s = [u, w]^T$ thus gives the image coordinates. All this is visualized in Fig.5. Thanks to the pinhole assumption

$$k \begin{bmatrix} x & y & z \end{bmatrix}^T = \begin{bmatrix} u & w & \lambda \end{bmatrix}^T, \tag{5}$$

we have that

$$u = \lambda \frac{x}{z}, \quad w = \lambda \frac{y}{z}. \tag{6}$$

To make this story complete, the coordinates in the image plane should then be quantized and the origin should be moved to the lower left corner to obtain pixel coordinates $[r, c]^T$

$$-\frac{u}{s_x} = (r - o_r), \quad -\frac{w}{s_y} = (c - o_c), \tag{7}$$

where s_x and s_y are the pixel dimensions and o_r and o_c are half the width and height of the image frame in pixels.

Nonetheless, for the analysis in this paper we will stick to u and w variables to make the formulas less involved. In simulations and experiments presented here, the "pixelized" information will be considered centered (again, in the name of simplicity). That is, we will use

$$-\frac{u}{s_x} = r, \quad -\frac{w}{s_y} = c. \tag{8}$$

The computer vision system that processes the images captured by the camera can surely perform this centering before sending the data to the pointing-tracking controller.

3.2 Camera motion and the interaction matrix

This subsection is again extracted from the nice introduction to image-based visual servoing in the textbook [8]. Consider the movement of the camera in the inertial space characterized by its linear and rotational velocities $v_C = [v_{Cx}, v_{Cy}, v_{Cz}]^T$ and $\omega_C = [\omega_{Cx}, \omega_{Cy}, \omega_{Cz}]^T$, both expressed in the camera frame. Stack them together to form a time-dependent vector $\xi(t) = [v_C(t), \omega_C(t)]^T \in \mathbb{R}^6$. To be rigorous, we should write $\omega^C_{R,C}$ to emphasize that it is an angular rate of the camera frame with respect to the reference (inertial) frame, expressed in the camera frame, and similarly $v^C_{o_C}$ to emphasize that it is a translational velocity of the origin o_C of the camera coordinate frame with respect to the inertial frame, also expressed in the camera frame. But this would yield the equations illegible.

The motion of the object as viewed by the camera is described by the so-called image feature velocity $\dot{s}(t)$, which can be obtained as a derivative of the image feature vector (in the simplest case it is just a position of some significant point). The nice thing is that it is possible to relate ξ and $\dot{s}$ by a transform resembling the concept of Jacobian and denoted often an interaction matrix or image Jacobian

$$\dot{s}(t) = L(s, z, \lambda)\xi(t). \tag{9}$$

Next we consider the simplest case of a single-point feature and assume that the ground object does not move. Extension of the results stated here to the case of a moving ground target is feasible, but the resulting interaction matrix will be a function of the velocity of the ground object, which is unknown to the inertial stabilization system (but it may be worth exploring if at least rough estimate of the object velocities can be used). This matrix is derived in [8], page 415, equation (12.14) as

$$\begin{bmatrix} \dot{u} \\ \dot{w} \end{bmatrix} = \begin{bmatrix} -\frac{\lambda}{z} & 0 & \frac{u}{z} & \frac{uw}{\lambda} & -\frac{\lambda^2+u^2}{\lambda} & w \\ 0 & -\frac{\lambda}{z} & \frac{w}{z} & \frac{\lambda^2+w^2}{\lambda} & -\frac{uw}{\lambda} & -u \end{bmatrix} \begin{bmatrix} v_{Cx} \\ v_{Cy} \\ v_{Cz} \\ \omega_{Cx} \\ \omega_{Cy} \\ \omega_{Cz} \end{bmatrix}. \tag{10}$$

The procedure for the derivation is straightforward: first, express the position of a fixed (not moving) point on the ground in the coordinate frame of the moving (rotating and translating) camera, and then project these new coordinates to the image plane. (It is vital to keep in mind within which coordinate frame the velocity vectors are being expressed. This is quite tedious. In this case, both the translational and rotational velocities are indeed considered with respect to the inertial reference frame but are expressed in the camera frame).

It appears useful to highlight the structure in the interaction matrix by writing it as a composition of two parts

$$\dot{s} = L_v(u, w, z)v_C + L_\omega(u, w)\omega_C, \tag{11}$$

because it turns out that only the part corresponding to the translation of the camera coordinate frame depends on the image depth (distance to the observed ground object) z. The rotational part is independent of z. The focal length λ is regarded as a fixed parameter.

The three components ω_{Cx}, ω_{Cy} and ω_{Cz} define the inertial angular rate vector $\omega_C = \left[\omega_{Cx}, \omega_{Cy}, \omega_{Cz}\right]^{\mathrm{T}}$ in the camera coordinate frame [C], which is rotated with respect to the elevation gimbal frame [E] using a fixed (constant) rotation matrix R_C^E

$$\omega_E = R_C^E \omega_C = \begin{bmatrix} 0 & 0 & 1 \\ -1 & 0 & 0 \\ 0 & -1 & 0 \end{bmatrix} \omega_C. \tag{12}$$

While by using the two direct drive motors it is possible, at least partially, to affect the vector ω_E by commanding its two components $\omega_{Ey}(=\omega_{\mathrm{EL}})$ and $\omega_{Ez}(=\omega_{\mathrm{CEL}})$, it is rather unlikely that the translational velocity v_C will be commanded by the autopilot based on the needs of the pointing-tracking algoritm. (But some projects might allow it).

Therefore, in order to develop some insight into the model, forget v_C for a moment (assume $v_C = 0$ temporarily, it can be treated as a disturbance later, either estimated or not). Using the transformation (12) and the rotation part of the interaction matrix (10) we get

$$\begin{bmatrix} \dot{u} \\ \dot{w} \end{bmatrix} = \begin{bmatrix} -\frac{uw}{\lambda} & \frac{\lambda^2+u^2}{\lambda} - w\tan\theta \\ \frac{\lambda^2+w^2}{\lambda} & \frac{uw}{\lambda} + u\tan\theta \end{bmatrix} \begin{bmatrix} \omega_{\mathrm{EL}}^{\mathrm{ref}} \\ \omega_{\mathrm{CEL}}^{\mathrm{ref}} \end{bmatrix} \tag{13}$$

and the camera tilt angle θ evolves according to

$$\dot{\theta}(t) = \omega_{\mathrm{EL}}^{\mathrm{ref}}(t). \tag{14}$$

3.3 Linearization at distinguished operating points

In order to develop an insight into the model (13), consider the situation when $\theta = 0$ (a wing-level flight and the camera pointing towards the horizon) and $w = 0$ (the observed object vertically centered on the screen). The dynamics is then constrained to one dimension and the equation simplifies to

$$\dot{u} = \frac{\lambda^2 + u^2}{\lambda}\omega_{\mathrm{CEL}}^{\mathrm{ref}}. \tag{15}$$

The term $(\lambda^2 + u^2)/\lambda$ expresses the nonlinear relationship between the angle and the line segment in the image plane. This is illustrated in Fig.6

The focal length λ for the system used by the authors ranges in $[4.2, 42]$ mm. The width of the CCD camera chip is 3.2 mm. Hence, for the maximum zoom, the nonlinear term can be approximated by λ even for u approaching the maximum value, that is, the observed objects is initially located near the borders of the field of view (and the control goal is to bring it to the center). The linear dynamics is then

$$\dot{u} = \lambda\omega_{\mathrm{CEL}}^{\mathrm{ref}}, \tag{16}$$

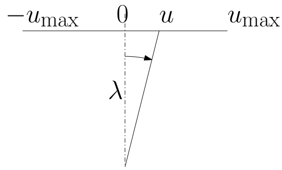

Figure 6: Relationship between the image coordinate system and the corresponding angle

that is, the model of dynamics is represented by a pure integrator with a gain λ (given by the optics). For shorter focal lengths (approaching the lower limit of 4.2 mm) this approximation is only valid for correspondingly smaller u, that is, for tracking purposes only, not for (re)pointing over a large part of the image plane.

3.4 Achievable bandwidth for pointing and tracking

The computer vision system works at discrete time instants with the sampling period T_s ranging between something like 0.1s and 2 s (depending on complexity and performance of the algorithm), which is relatively long compared to 250 Hz of the inner inertial rate loop. This introduces a total delay τ of about $1.5T_s$ into the feedback loop.

It is known that the achievable bandwidth is limited by several properties of the system, delay being one of them. With the sampling period of the image tracker set to $T_s = 0.5\,s$, the achievable bandwidth is approximately limited by

$$\omega_{\mathrm{BW}} < \frac{1}{\tau} = \frac{1}{1.5T_s} = 1.3\,\mathrm{rad}/s = 0.2\,\mathrm{Hz}. \tag{17}$$

It is derived in [12] from ideal closed-loop transfer functions achievable for systems with a delay τ. Ideally, $T(s) = 1e^{-\tau s}$, therefore $S(s) = 1 - e^{-\tau s}$. By Taylor series expansion $S(s) \approx \tau s$. Therefore $|S(j\omega)|$ crosses 0 dB at about $1/\tau$.

This suggests that the fastest possible pointing-tracking loop will work up to a fraction of 1 Hz if the information from the image tracker is provided twice per second and is delayed one sample period. This

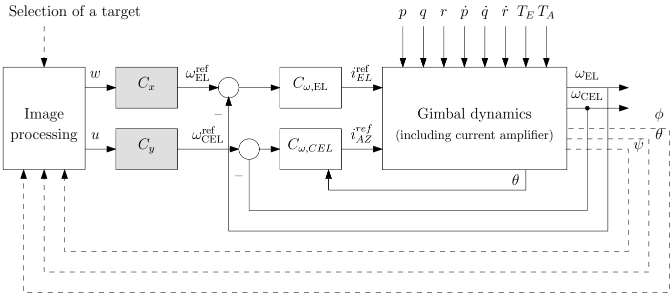

Figure 7: Naive pointing-tracking system formed by two SISO loops closed around two inertial rate stabilization loops. The dashed lines are not signals truly fed back to the pointing-tracking controller. These are variables representing orientation of the camera which affects the position and orientation of objects in the image plane.

roughly corresponds to the classical rule-of-thumb rules [13] for selection of a sampling rate for undelayed systems as 10 to 20 times the closed-loop bandwidth.

4 Decoupled pointing and tracking

Proceeding one step further beyond the mere inertial stabilization, the question of the most suitable feedback control configuration for automatic visual tracking pops up. Shall we use the immediate extension which closes a SISO tracking loop around the corresponding SISO inertial rate loop?

The cascade approach is justified: whereas the inner (inertial rate) loop aims to attenuate the disturbances at middle and high frequencies, the outer (pointing) loop should be active at low frequencies. This straightforward but naive solution is in Fig.7.

Insisting on decoupled controllers is plausible from an implementation viewpoint. There is a trick hidden here, though, as seen in Fig.8. When the automatic computer vision tracker detects a regulation error in the horizontal direction in the image plane while seeing no error in

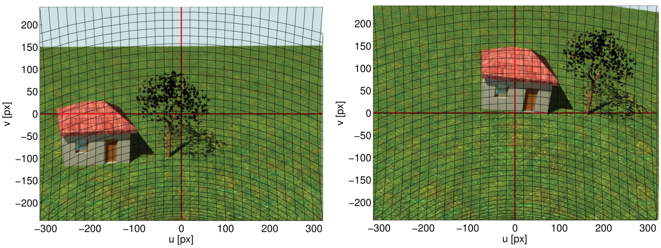

Figure 8: Illustration of how in an attempt to steer the camera such that the image of the roof of the house gets back to the middle of the field of view using azimuth motor only, the introduced rotation of the camera around its optical axis makes the horizontal movement curved. Consequently, correction in vertical direction using the elevation motor is needed. Curvilinear coordinate system in the image plane corresponds to the initial elevation of camera by $\theta = -54°$ with respect to the body of the aircraft.

vertical direction, the simple cascaded structure of Fig.7 would command the azimuth motor only. This motor alone, however, cannot create a purely horizontal motion in the image plane when $\theta \neq 0$. A geometric explanation can be found in Fig.1: to steer the camera such that the image of an object moves horizontally in an image plane, one would need to command the cross-elevation inertial rate ω_{CEL} (denoted as ω_{Ez} in the figure). However, the motor can only affect the component of the inertial rate in the direction of the azimuth motor axis, that is, ω_{Az}. As soon as there is some misalignment between the two, that is, when the camera is tilted up or down to the ground while the aircraft is in level flight ($\theta \neq 0$), the vector oriented in the azimuth motor axis of length ω_{Az} has some nonzero projection ω_{Ex} to the camera optical axis. Consequently, some unwanted rotation of the image as well as vertical displacement are introduced. Curvilinear coordinate mesh in Fig.8 is generated by the nonlinear dynamics (13).

However, with sampling rate of the outer (image-based pointing-tracking) loop fast enough, the error introduced by the coupling between the two camera axes would be corrected in the very next step, when the regulation error in vertical direction in the image plane is detected and a correcting command to the elevation motor would be sent. The currently implemented prototype system achieves sampling rate of 15 Hz, which seems enough to justify this naive approach. Having scanned the available literature, the authors can only suspect that some of the available commercial systems follow this approach too. The motivation for this paper is to improve this scheme, because a bit more advanced and computationally intensive computer vision algorithms can slow down the sampling rate of the outer loop to something like 1 or 2 s.

5 Feedback linearization for pointing & tracking

The key idea for an improvement described in the rest of the paper is that the curvature of the coordinate axes as in Fig.8 can be compensated for by measuring the third component of the inertial angular rate of the camera body, the one along its optical axis, the so far unused measurement ω_{Ex}. It is available at the sampling rate a few orders of magnitude faster than what the computer vision system provides. Using this information, exact feedback linearization can be implemented in the controller following standard techniques from image-based visual servoing introduced next.

The idea behind image-based visual servoing is that an error "sensed" in the image plane by the image tracker as

$$e(t) = s(t) - s^{\mathrm{ref}} \tag{18}$$

can be eliminated by commanding a proper value of $\xi(t)$, which characterizes the velocity of the camera frame. Note that $s^{\mathrm{ref}} = 0$ when the task is to bring the image of the object into the central position in the image plane by pushing $s(t) = [u(t), w(t)]^T$ to zero. How to find a proper ξ? Simply by inverting the interaction matrix L. In the case of a single-point feature, the matrix is 2×6, which suggests that such a solution will not be unique. Which one to pick? It will be shown shortly that there is one important constraint here which makes only one solution acceptable.

In contrast to common robotics tasks, here we cannot influence the translational position of the camera frame (unless there is a bidirectional communication between the UAV autopilot and the inertial stabilization & visual tracking system). Hence the linear velocity $v_C = [v_{Cx}, v_{Cy}, v_{Cz}]^T$ of the camera coordinate origin needs to be taken as given (enforced) from the outside. But then the task of determining ξ at a given time instant consists in solving the linear system (10) with the term corresponding to translation moved to the right-hand side

$$L_\omega(u,w)\omega_C = \dot{s} - L_v(u,w,z)v_C. \tag{19}$$

The 2×3 matrix L_ω has a 1-dimensional nullspace parameterized by

$$\mathcal{N} = \{\omega_c = k \begin{bmatrix} u & w & \lambda \end{bmatrix}^T\}, \tag{20}$$

which can be interpreted quite intuitively: rotating the camera about the line connecting the observed point and the origin of the camera frame does not contribute to a change of the coordinates of the point in the image plane. With the right pseudoinverse of L_ω given by

$$L_\omega^\sharp = \begin{bmatrix} 0 & \frac{\lambda}{\lambda^2+u^2+w^2} \\ -\frac{\lambda}{\lambda^2+u^2+w^2} & 0 \\ \frac{w}{\lambda^2+u^2+w^2} & -\frac{u}{\lambda^2+u^2+w^2} \end{bmatrix}, \tag{21}$$

all solutions are parametrized by a single constant k

$$\omega_C = L_\omega^\sharp \dot{s} - L_\omega^\sharp L_v v_C + k \begin{bmatrix} u & w & \lambda \end{bmatrix}^T. \tag{22}$$

Substituting and abusing k since it is arbitrary we get

$$\omega_C = \frac{1}{z\left(\lambda^2+u^2+w^2\right)} \begin{bmatrix} \lambda^2 v_y - \lambda v_z w + \lambda \dot{w} z + ku \\ -\lambda^2 v_x + \lambda v_z u - \lambda \dot{u} z + kw \\ -\lambda u v_y + \lambda w v_x - u \dot{w} z + \dot{u} w z + k\lambda \end{bmatrix}. \tag{23}$$

What we have obtained so far is a procedure which for given velocities $\dot{u}$ and $\dot{w}$ of a point feature in the image plane computes the required angular velocity vector ω_C (it does not hurt now to use the full notation $\omega_{R,C}^C$) of the camera. A single arbitrary parameter k can be used to give some choice, which is the key idea to be exploited next.

5.1 Proportional image-based pointing and tracking

In order to pull $s(t)$ to the vicinity of $(0, 0)$ in the image plane, a cascade control structure can be used: the pointing-tracking controller sets the reference rate vector $\dot{s}^{\mathrm{ref}}(t)$ such that its actual value $s(t)$ goes to zero. One simple approach is to require exponential stability, that is, both $u(t)$ and $w(t)$ go to zero values according to

$$\dot{s}(t) = As(t), \tag{24}$$

where A has nonnegative eigenvalues. The simplest solution can be obtained by restricting A to a diagonal matrix $A = -\alpha I$ for some real positive α and then

$$\dot{s}(t) = -\alpha s(t). \tag{25}$$

The larger the α, the faster the error in the image plane goes to zero. Practical considerations of the choice of this parameter are discussed at the end of this section. Now, how can we force this error to evolve as in (25)? Noting that $\dot{s}(t)$ is related to the camera inertial angular velocities according to (23), we can conclude that asymptotically stable image error is guaranteed if the camera inertial velocities follow the reference value

$$\omega_C^{\mathrm{ref}} = \frac{1}{z\left(\lambda^2 + u^2 + w^2\right)} \begin{bmatrix} \lambda^2 v_y - \lambda v_z w - \lambda \alpha w z + k u \\ -\lambda^2 v_x + \lambda v_z u + \lambda \alpha u z + k w \\ -\lambda u v_y + \lambda w v_x + k \lambda \end{bmatrix}. \tag{26}$$

It is not clear at this moment whether and how such a rotation rate of the camera can be established by the two motors. It is the free parameter k that can help to pick such a reference inertial velocity vector ω_C^{ref} of the camera that is realizable by the two motors.

5.2 Establishing the camera rate using two motors

Once we know the required inertial angular rate of the camera, what remains is to express it via constant transformation R_C^E in the inner gimbal frame

$$
\begin{aligned}
\omega_E^{\text{ref}} &= R_C^E \omega_C^{\text{ref}} \\
&= \frac{1}{z\left(\lambda^2+u^2+w^2\right)} \begin{bmatrix} -\lambda u v_y + \lambda w v_x + k\lambda \\ -\lambda^2 v_y + \lambda v_z w + \lambda \alpha w z - k u \\ \lambda^2 v_x - \lambda v_z u - \lambda \alpha u z - k w \end{bmatrix}.
\end{aligned} \tag{27}
$$

The task for the inertial angular rate control system is to follow this velocity by commanding the two motors. It is important to keep track of the corresponding frames. The resulting ω_E^{ref} is fully labeled as $\omega_{R,E}^{E,\text{ref}}$ as it gives the required inertial rotation rate of the inner gimbal. Its true value is measured by the three-axis MEMS gyro fixed to the inner gimbal.

Now comes the key part. Having only two motors, it is not possible to set all the three components of the vector of inertial angular velocity independently. But the free scalar parameter k can be used to pick a specific triple that requires no change with respect to the current value of ω_{Ex} (inertial angular rate of the camera around its optical axis). The value of ω_{Ex} must be available to the controller then. Solving (27) for the value of k guaranteeing that the x component of the vector on the right is equal to the measured ω_{Ex} gives

$$
k = -w v_x + u v_y + \frac{z\left(\lambda^2+u^2+w^2\right)}{\lambda}\omega_{Ex}. \tag{28}
$$

Substituting this value back to the expressions for the other two components of the reference angular rate vector, the expressions for the controller outputs follow

$$
\begin{aligned}
\omega_{\text{EL}}^{\text{ref}} = \omega_{Ey}^{\text{ref}} &= \frac{\alpha w \lambda}{\lambda^2+u^2+w^2} - \frac{\omega_{Ex} u}{\lambda} \\
&\quad - \frac{\lambda^2 v_y - \lambda w v_z - u w v_x + u^2 v_y}{z(\lambda^2+u^2+w^2)},
\end{aligned} \tag{29}
$$

$$
\begin{aligned}
\omega_{\text{CEL}}^{\text{ref}} = \omega_{Ez}^{\text{ref}} &= -\frac{\alpha u \lambda}{\lambda^2+u^2+w^2} - \frac{\omega_{Ex} w}{\lambda} \\
&\quad + \frac{\lambda^2 v_x - \lambda u v_z - w u v_y + w^2 v_x}{z(\lambda^2+u^2+w^2)}.
\end{aligned} \tag{30}
$$

The expressions (29) and (30) for the controllers are structured such

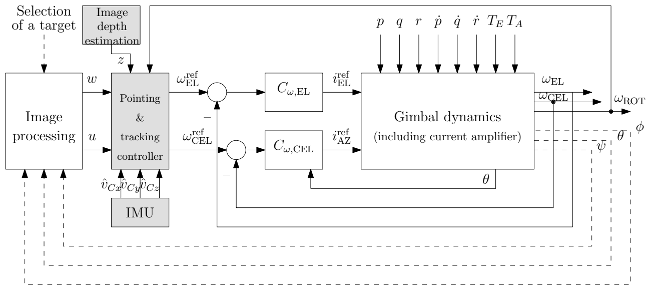

Figure 9: Full feedback system with an image-based pointing controller aware of the angular rate about the optical axis and the translational motion

that three terms can be immediately recognized in each controller: a term corresponding to a regulation error in the corresponding axis as seen in the image plane, a term compensating for the rotation around the camera optical axis and finally a term attenuating the influence of mutual translational motion of the camera and the ground object.

In order to get an insight into this new controller and compare it with the originally proposed decoupled one, consider again the easy situation when the carrier is in level flight and the camera is pointing towards the horizon ($\theta = 0$). Neglect the translational velocities v_C. The observed object is vertically centered in the image plane, that is, $w = 0$. The expressions in (29) and (30) simplify to

$$\omega_{Ey}^{\mathrm{ref}} = 0, \tag{31}$$

$$\omega_{Ez}^{\mathrm{ref}} = -\alpha \frac{\lambda}{\lambda^2 + u^2} u. \tag{32}$$

Compare this simplified controller and the model of the system (15) valid for the same conditions. Apparently, the nonlinear term $\lambda/(\lambda^2 + u^2)$ serves just to invert the nonlinearity in the model. And this is what the controller does in general. It inverts the nonlinearity. In other words, it performs feedback linearization. Consideration of the inertial angular rate ω_{Ex} of the camera around its optical axis is another measure that the controller takes to invert the nonlinearity. For the maximum zoom ($\lambda = 42mm$), the nonlinear term $\lambda/(\lambda^2 + u^2)$ is sufficiently close to λ and therefore the controller's action is driven by

$$\omega_{Ez}^{\text{ref}} = -\alpha \frac{1}{\lambda} u. \tag{33}$$

The simplification can take place even in a more general situation $u, w \neq 0$ but small, and λ large (and v_C still neglected). The general expression for the controller output then reduces to

$$\omega_{Ey}^{\text{ref}} = \frac{\alpha w}{\lambda} - \frac{\omega_{Ex} u}{\lambda} \tag{34}$$

$$\omega_{Ez}^{\text{ref}} = -\frac{\alpha u}{\lambda} - \frac{\omega_{Ex} w}{\lambda} \tag{35}$$

This reduced controller reveals the key enhancement with respect to the fully decoupled design: the controller output contains contribution from the angular rate of the camera around the optical axis!

5.3 Controller structure for pointing and tracking

The feedback-linearizing pointing-tracking controller in (29) and (30) does not preserve the decoupled structure (no longer two separate pointing-tracking controllers). Each of the two controllers accepts not only both the "measured" position errors, that is, u and w, but also

1. the x-component of the vector ω_E describing the inertial angular rate of the camera around the optical axis,
2. estimates of the aircraft translational velocity with respect to the ground, expressed in the camera coordinate frame (v_{Cz} describes how fast the camera is approaching the target),
3. an estimate of depth z of the image, that is, the distance from the camera to the ground target.

Moreover, the technical parameter that the controller must be aware of is the focal length λ. An upgrade of the naive scheme proposed in Fig.7 can thus be seen in Fig.9.

The key challenge in implementing this controller fully is in providing the controller with the extra measurements and/or estimates of the three components of the translational velocity v_C and the distance z to the object. These could be approached using inertial measurement unit (IMU) in combination with a laser range-finder and possibly also in combination with a computer vision system. For instance, the depth z and the "towards the object" velocity v_{Cz} is sometimes estimated from the apparent size of an object in the image (covering the image of the object by some polygon and computing its area, which is suggested in [8]). This technique can turn out of limited use here, though, because the images of observed objects can span just a few pixels and determination of v_{Cz} is then very inaccurate.

On the other hand, these new "complications" caused by the requirements of measuring the translational velocities are not really new and tied to the proposed control scheme. They are equally valid even with the (naive) decoupled control. Unless the translation velocity is known, one simply cannot tell whether the image is moving due to undamped aircraft oscillations or because the aircraft is approaching the object. But now, with the systematic analysis documented in this paper, the structure of the ideal controller is known. It is up to an engineer to decide whether or not to ignore the translational motion and regard its effects as unmeasured disturbance. Such disturbance is only significant at low frequencies and can be left for the image-based pointing loop to attenuate.

6 Laboratory experiments

The platform introduced in the report was used to validate the proposed control scheme and compare its performance with the intuitive decoupled controller. The experimental test was conducted in an indoor lab while the camera platform was carried by a fixed laboratory stand. Therefore it was only the objects on the ceiling rather than on the floor that could be tracked conveniently. Both the new and the original (naive) decoupled controllers were tested only for the faster sampling rate of 15 Hz of the automatic image tracker. The controllers already included the simple heuristic delay compensation described elsewhere (although it was not much needed with this fast sampling rate).

The bandwidth of the inertial rate loop can be experimentally demonstrated to be at least 1 Hz, see Fig.10. Therefore the assumption that the rate loop guarantees tracking of the required inertial rates up to a fraction of Hz is satisfied.

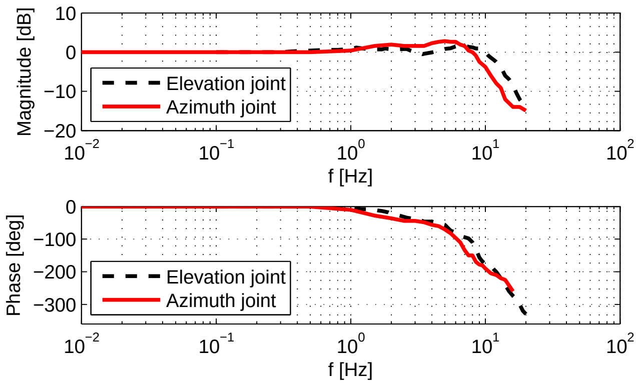

Figure 10: Measured frequency responses for both inertial rate loops. The required inertial rate as an input and the true (measured) inertial rate as an output. The amplitude of the reference inertial rate was set up to 7.3°/s.

Several experiments were conducted and the measurements from one of them are visualized here in Fig.11, the experimental data for the new algorithm always on the left and the data for the original decoupled scheme on the right. The experiment validates the pointing and tracking performance even in presence of a disturbing rotational motion of the carrier. Namely, the optical axis of the camera was initially pointing to the ceiling with the elevation $\theta(0) = 70°$ and the laboratory stand was rotated manually around its vertical axis (orthogonal to the surface of the desk).

7 Conclusions

We presented a systematic procedure for designing and implementing a pointing and tracking image-based controller for an airborne camera platform with an inertial line-of-sight stabilization already designed and implemented. The proposed scheme uses extra information from an inertial angular rate sensor; namely, the angular velocity of the payload (camera, laser) around its optical axis. This extra measurement

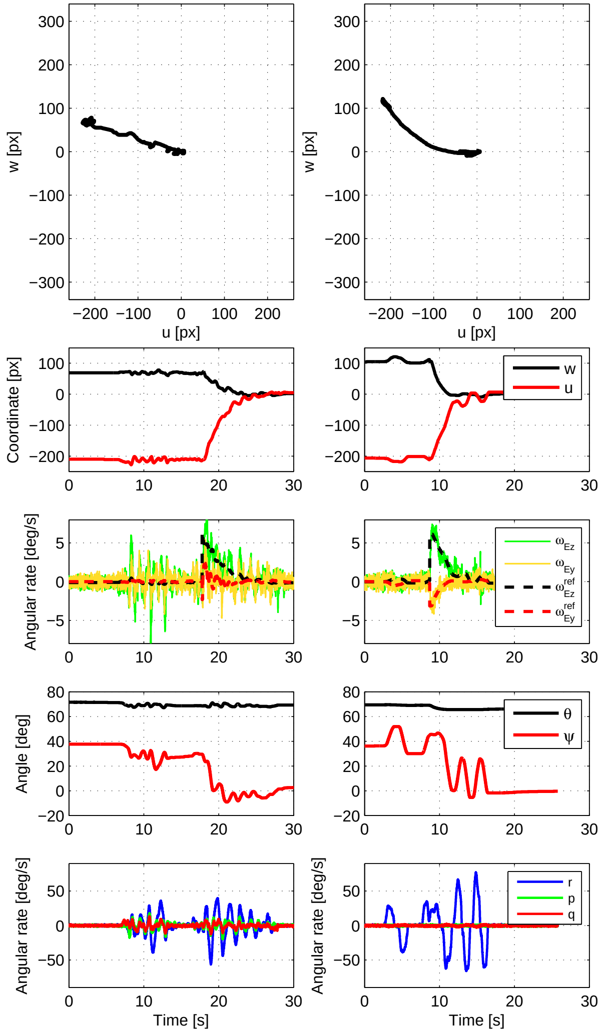

Figure 11: Experiment: Responses of relevant quantities for the pointing exposed to external (recorded) disturbances p, q, r. $\theta(0) = 70°$, tracker sampling rate $f_{\rm sp} = 15$Hz, $\alpha = 0.46$. Left: the proposed algorithm, right: the decoupled approach.

is provided by a MEMS gyro at a much faster sampling rate than the pointing-tracking error produced by a computer vision system. Moreover, the proposed controller can take into consideration the measured or estimated translation velocity of the aircraft with respect to the observed target (to compensate for the paralactic phenomenon).

The essence of the proposed design technique is that of a feedback linearization. The resulting controller enforces linear dynamics in the image plane. This not only makes the analysis and design systematic but putting it on the well-explored ground, but also makes the response of the system a bit more friendly for a human operator as the system follows linear paths in the image plane during (re)pointing.

The proposed scheme was thoroughly simulated and verified by practical laboratory experiments with a realistic benchmark system and compared against the more intuitive decoupled control scheme. Possible simplifications were discussed and practical pitfalls were highlighted.

References

[1] M. Masten and L. Stockum, Eds., *Selected Papers on Precision Stabilization and Tracking Systems for Acquisition, Pointing and Control Applications*, ser. SPIE Milestone Series, vol. MS 123. Bellingham WA: SPIE, 1996.

[2] M. Masten, "Inertially stabilized platforms for optical imaging systems: Tracking dynamic dynamic targets with mobile sensors," *Control Systems Magazine, IEEE*, vol. 28, pp. 47–64, Feb. 2008.

[3] J. M. Hilkert, "Inertially stabilized platform technology: concepts and principles," *Control Systems Magazine, IEEE*, vol. 28, pp. 26–46, Feb. 2008.

[4] J. Debruin, "Control systems for mobile satcom antennas," *Control Systems Magazine, IEEE*, vol. 28, no. 1, pp. 86–101, Feb. 2008.

[5] J. Osborne, G. Hicks, and R. Fuentes, "Global analysis of the double-gimbal mechanism," *Control Systems Magazine, IEEE*, vol. 28, no. 4, pp. 44–64, aug 2008.

[6] Z. Hurák and M. Řezáč, “Combined line-of-sight inertial stabilization and visual tracking: application to an airborne camera platform,” in *Proc. of the 48th IEEE Conference on Decision and Control*, Shanghai, China, December 2009.

[7] ——, “Control design for image tracking with an inertially stabilized airborne camera platform,” in *Proc. of SPIE Deference, Security, and Sensing 2010*, Orlando, Florida, USA, April 2010.

[8] M. W. Spong, S. Hutchinson, and M. Vidyasagar, *Robot Modeling and Control*. Wiley, 2006.

[9] A. Rue, “Stabilization of precision electrooptical pointing and tracking systems,” *Aerospace and Electronic Systems, IEEE Transactions on*, vol. AES-5, no. 5, pp. 805–819, Sep. 1969.

[10] ——, “Precision stabilization systems,” *Aerospace and Electronic Systems, IEEE Transactions on*, vol. AES-10, no. 1, pp. 34–42, Jan. 1974.

[11] F. Chaumette and S. Hutchinson, “Visual servo control, part I: Basic approaches,” *Robotics & Automation Magazine, IEEE*, vol. 13, no. 4, pp. 82–90, Dec. 2006.

[12] S. Skogestad and I. Postlethwaite, *Multivariable Feedback Control: Analysis and Design*, 2nd ed. Wiley, Nov. 2005.

[13] G. F. Franklin, J. D. Powell, and M. L. Workman, *Digital Control of Dynamic Systems*, 3rd ed. Prentice Hall, Dec. 1997.

Ing. Zdeněk Hurák, Ph.D. (*May 15, 1974)

Education

- 2000-2004: **Ph.D.** degree. Department of Control Engineering, Faculty of Electrical Engineering, Czech Technical University in Prague. Supervisor: Prof. Michael Šebek. Thesis title: *ℓ_1-optimal control - a polynomial approach.* The key result published in the prestigious *SIAM Journal on Control and Optimization.*

- 1992-1997: **Ing.** degree ($\approx$ M.Sc. or Dipl.Ing.), with honors. Dept. of Aerospace Electrical Engr., University of Defense (formerly Military Academy) in Brno, Czech Republic. Major specialization in avionics and weapon systems.

Affiliation

- 2000–present: Faculty of Electrical Engr., Czech Technical University in Prague, Czech Republic. Includes also the Ph.D. years through the involvement in *Center for Applied Cybernetics* project. Since 2009 **assistant professor**, establishing his *Advanced Algorithms for Control and Communications* research group: `http://aa4cc.dce.fel.cvut.cz` within Dept. of Control Engineering.

- 2000–2006: part-time researcher at Institute of Information Theory and Automation, Czech Academy of Sciences, Prague.

- 1997–1999: teaching and lab assistant at Dept. of Aerospace Electrical Engr., Military Academy in Brno, Czech Republic.

Scholarships and visiting positions abroad

- Fulbright scholar at Dept. of Mech. Engineering and Center for Control, Dynamical Systems and Computation, College of Engineering, University of California, Santa Barbara, USA. Hosted by Prof. Bassam Bamieh. February through August 2014. Research in distributed control of distributed systems.

- Visiting researcher at Micro and Nano Scale Engineering group (MNSE), Dept. of Mech. Eng., TU Eindhoven, The Netherlands.

Hosted by Prof. Yves Bellouard. May through December 2008. Setting up an experimental platform for dielectrophoresis-based micromanipulation.

- Boeing research fellow at International Institute of Theoretical and Applied Physics, Iowa State University, Ames, USA. March through June 1999. Research in control and scheduling.

Membership and activities in professional societies

- Senior Member of IEEE: Control Systems Society (member for 15 years) and Robotics and Automation Society, Chair of Control System Chapter of Czechoslovak Section of IEEE. See `http://control.ieee.cz` (in Czech).

- Editorial boards: Kybernetika `http://www.kybernetika.cz` (2008-2014), Automa `http://www.automa.cz`.

- Member of IPC of 2011 IEEE Multi-Conference on Systems and Control, September 28-30, 2011, Denver, CO, USA. Member of IPC of 7th International Workshop on Multidimensional (nD) Systems (nDS11), September 5-7, 2011, Poitiers, France.

Research projects

- Bio-inspired Assembly Process for Mesoscale Products and Systems. EC FP6 (STREP). Participation in a consortium lead by Dr. Yves Bellouard (TU Eindhoven, The Netherlands). Duration: 2006–2009. Managing 3 researchers (36 person-months). The team budget: 160 000 EUR.

- Center of Excellence for Advanced Bioanalytical Instrumentation. GAČR. Jointly with two other research labs (chemistry and biochemistry). Duration: 2012–2018. Managing research of 3 researchers, bringing in a foreign postdoctoral researcher. The team budget: 18.5 mil. CZK. Web: `http://www.biocentex.cz`.

Industrial collaboration

- Design of several versions of a line-of-sight stabilization for an airborne camera system. Contractor/partner: Czech Air Force R&D Institute (VTÚL `http://vtul.cz`). Other partners: prof. Václav Hlaváč's Center for Machine Perception, ESSA company. Responsible for the inertial stabilization subsystem; managing a small team of control engineers (past graduates). 2006–2014.

- Courses on *Automatic control* for industry: Honeywell Technology Solutions Lab, Brno, Czech Republic, 12 lectures, January 2008; STMicroelectronics Prague, 6 lectures, 2016.

- Robust control design for the Very Large Telescope (8.2m VLT). Contractor: European Southern Observatory, Santiago, Chile. Consulting for an ESO control engineer (Toomas Erm), using $\mathcal{H}_\infty$ norm minimization based loop-shaping for increasing the bandwidth of the altitude control system. 2003.

- Reliability analysis of the PLAMEN fire control system for the L-159 aircraft: FMEA, FMECA and FTA analyses, simulations, MIL-HDBK-217. Contractor: AEV, Ltd., Kromeriz. 1998.

Scientific awards

- 4th place at *2012 NIST Mobile Microrobotics Challenge* during IEEE ICRA, May 2012, St.Paul, MN, USA. Then 5th place at *2013 IEEE RAS Mobile Microrobotics Challenge* during IEEE ICRA, May 2013, Karlsruhe, Germany.

- Prize of the Rector of Czech Technical University for an outstanding research paper (Minimum distance to the range...) of the year 2006. Best paper (Robust stability of polynomials with complex coefficients) at an international student conference POSTER 2001, Prague, May 2001 (Czech Airlines prize).

Research publication activities

Author or coauthor of **13 papers** (and one editorial-type of a contribution) in **journals** indexed in SCI or SCI Extended. Above 20 papers at refereed international conferences (mostly organized by IEEE and IFAC). **H-index** is **5** according to Web of Science (WoS), **5** according to Scopus, and **9** according to Google Scholar. The total number of **citations** (without self-citations) is **68** according to WoS, **71** according to Scopus, and **315** according to Google Scholar (self-citations not excluded). ResearcherID: C-8373-2009.

SCI journal papers

[1] P. Augusta and Z. Hurák, "Distributed stabilisation of spatially invariant systems: positive polynomial approach," *Multidimensional Systems and Signal Processing*, pp. 1–19, 2013.

[2] O. Šprdlík, Z. Hurák, M. Hoskovcová, O. Ulmanová, and E. Růžička, "Tremor analysis by decomposition of acceleration into gravity and inertial acceleration using inertial measurement unit," *Biomedical Signal Processing and Control*, vol. 6, no. 3, pp. 269–279, 2011.

[3] M. Řezáč and Z. Hurák, "Structured MIMO design for dual-stage inertial stabilization: Case study for HIFOO and Hinfstruct solvers," *Mechatronics*, vol. 23, no. 8, pp. 1084–1093, Dec. 2013.

[4] M. Špiller and Z. Hurák, "Hybrid charge control for stick–slip piezoelectric actuators," *Mechatronics*, vol. 21, no. 1, pp. 100–108, 2011.

[5] B. Cichy, P. Augusta, E. Rogers, K. Gałkowski, and Z. Hurák, "Robust control of distributed parameter mechanical systems using a multidimensional systems approach," *Bulletin of the Polish Academy of Sciences: Technical Sciences*, vol. 58, no. 1, pp. 67–75, Mar. 2010.

[6] B. Cichy, P. Augusta, E. Rogers, K. Galkowski, and Z. Hurak, "On the control of distributed parameter systems using a multidimensional systems setting," *Mechanical Systems and Signal Processing*, vol. 22, no. 7, pp. 1566–1581, 2008.

[7] Z. Hurák, M. Hromčík, and M. Špiller, "Minimization of l2 norm of the error signal in posicast input command shaping: a poly-

nomial approach," *International Journal of Robust and Nonlinear Control*, vol. 17, no. 8, pp. 706–719, 2007.

[8] Z. Hurak, A. Böttcher, and M. Sebek, "Minimum Distance to the Range of a Banded Lower Triangular Toeplitz Operator in l1 and Application in l1-Optimal Control," *SIAM Journal on Control and Optimization*, vol. 45, no. 1, pp. 107–122, Jan. 2006.

[9] I. Herman, D. Martinec, Z. Hurak, and M. Sebek, "Nonzero Bound on Fiedler Eigenvalue Causes Exponential Growth of H-Infinity Norm of Vehicular Platoon," *IEEE Transactions on Automatic Control*, vol. 60, no. 8, pp. 2248–2253, Aug. 2015.

[10] J. Zemánek, T. Michálek, and Z. Hurák, "Feedback control for noise-aided parallel micromanipulation of several particles using dielectrophoresis," *ELECTROPHORESIS*, vol. 36, no. 13, pp. 1451–1458, 2015.

[11] Z. Hurák and F. Foret, "On benchmark problems, challenges, and competitions in electrokinetics—A review," *ELECTROPHORESIS*, vol. 36, no. 13, pp. 1429–1431, 2015.

[12] D. Martinec, I. Herman, Z. Hurák, and M. Šebek, "Wave-absorbing vehicular platoon controller," *European Journal of Control*, vol. 20, no. 5, pp. 237–248, Sep. 2014.

[13] B. Cichy, P. Augusta, E. Rogers, K. Gałkowski, and Z. Hurák, "Robust control of distributed parameter mechanical systems using a multidimensional systems approach," *Bulletin of the Polish Academy of Sciences: Technical Sciences*, vol. 58, no. 1, pp. 67–75, Mar. 2010.

[14] Z. Hurak and M. Rezac, "Image-Based Pointing and Tracking for Inertially Stabilized Airborne Camera Platform," *IEEE Transactions on Control Systems Technology*, vol. 20, no. 5, pp. 1146–1159, Sep. 2012.

Teaching experience

- Three Ph.D. candidates brought to a successful defense (Petr Augusta—2011, Otakar Šprdlík—2012, Martin Řezáč—2014). All finished defended with at least one paper in a good (SCI) journal. At least one opponent of the candidate's final thesis was from abroad.

- Currently advising three Ph.D. students: Jiří Zemánek, Martin Gurtner and Tomáš Michálek, and co-advising another: Ivo Herman. Ivo Herman submitted the thesis in May 2016.

- Supervised in total 27 final graduate (Ing/MSc) and 16 final undergraduate student projects.

- Created and taught a graduate course on *optimal and robust control*. See `https://moodle.fel.cvut.cz/course/view.php?id=418`. The course taught in English. Attendance: 10 through 20 students every year.

- Created and taught undergraduate course on *modeling and simulation of dynamic systems*. See `http://moodle.fel.cvut.cz`. On average 30 students every year. Sponsorship from an industrial companies used to provide the students with cca 40 copies of a worldwide used textbook. Implemented *flipped classroom*. Videolectures online on `https://www.youtube.com/user/aa4cc`.

- Member of the Council of the *Cybernetics and robotics* graduate program at FEE CTU in Prague. Contributing to setting up and running the program.